This document is the accepted manuscript version of the following article:
Johnson, T. J., Olfert, J. S., Symonds, J. P. R., Johnson, M., Rindlisbacher, T., Swanson, J. J., Boies, A. M., Thomson, K., Smallwood, G., Walters, D., Sevcenco, Y., Crayford, A., Dastanpour, R., Rogak, S. N., Durdina, L., Bahk, Y. K., Brem, B., & Wang, J. (2015). Effective density and mass-mobility exponent of aircraft turbine particulate matter. Journal of Propulsion and Power, 31(2), 573-582. https://doi.org/10.2514/1.B35367

Effective density and mass-mobility exponent of aircraft turbine particulate matter

Tyler J. Johnson[*] and Jason S. Olfert[†]
University of Alberta, Edmonton, Alberta, T6G 2G8, Canada

Jonathan P.R. Symonds[‡]
Cambustion Ltd., Cambridge, CB1 8DH, U.K.

Mark Johnson[§]
Rolls-Royce plc, Derby, DE24 8BJ, U.K.

Theo Rindlisbacher[**]
Swiss Federal Office of Civil Aviation, CH-3003 Bern, Switzerland

Jacob J. Swanson[††]
Minnesota State University, Mankato, Mankato, MN, 56001, United States

Adam M. Boies[‡‡]
University of Cambridge, Cambridge, CB2 1PZ, U.K.

Kevin Thomson[§§] and Greg Smallwood[***]
National Research Council Canada, Ottawa, Ontario, K1A 0R6, Canada

David Walters[†††], Yura Sevcenco[‡‡‡] and Andrew Crayford[§§§]
Cardiff University, Cardiff, CF24 3AA, U.K.

Ramin Dastanpour[****] and Steven N. Rogak[††††]
*University of British Columbia, Vancouver, British Columbia, V6T 1Z4, Canada*Lukas Durdina [‡‡‡‡], Yeon Kyoung Bahk [§§§§], Benjamin Brem[*****] and Jing Wang[†††††]

[*] Research Student, 2-11 Department of Mechanical Engineering, University of Alberta, Edmonton, Alberta, T6G 2G8, Canada.

[†] Assistant Professor, 5-01C Department of Mechanical Engineering, University of Alberta, Edmonton, Alberta, T6G 2G8, Canada.

[‡] R&D Director, Cambustion Ltd., J6 The Paddocks, 347 Cherry Hinton Road, Cambridge, CB1 8DH, U.K.

[§] Emissions Measurement Expert, Test and Measurement, Rolls-Royce plc, Derby, DE24 8BJ, U.K.

[**] Scientific Advisor, Swiss Federal Office of Civil Aviation, Environmental Section, CH-3003 Bern, Switzerland.

[††] Assistant Professor, Department of Integrated Engineering, Minnesota State University, Mankato, Mankato, MN, 56001, United States.

[‡‡] Lecturer, Division of Energy, Department of Engineering, University of Cambridge, Trumpington Street, Cambridge, CB2 1PZ, U.K.

[§§] Discipline Leader, Measurement Science and Standards, National Research Council Canada, Ottawa, Ontario, K1A 0R6, Canada.

[***] Program Leader, Measurement Science and Standards, National Research Council Canada, Ottawa, Ontario, K1A 0R6, Canada.

[†††] Research Student, GTRC, Cardiff University, School of Engineering, Cardiff, CF24 3AA, U.K.

[‡‡‡] Project Engineer, GTRC, Cardiff University, School of Engineering, Cardiff, CF24 3AA, U.K., and Member of AIAA.

[§§§] Lecturer, GTRC, Cardiff University, School of Engineering, Cardiff, CF24 3AA, U.K.

[****] Research Student, Department of Mechanical Engineering, University of British Columbia, Vancouver, British Columbia, V6T 1Z4, Canada.

[††††] Professor, Department of Mechanical Engineering, University of British Columbia, Vancouver, British Columbia, V6T 1Z4, Canada.

[‡‡‡‡] Research Student, Empa, Swiss Federal Laboratories for Materials Science and Technology, CH-8600 Dübendorf, Switzerland.

[§§§§] Research Student, Empa, Swiss Federal Laboratories for Materials Science and Technology, CH-8600 Dübendorf, Switzerland.

[*****] Research Associate, Empa, Swiss Federal Laboratories for Materials Science and Technology, CH-8600 Dübendorf, Switzerland.

[†††††] Assistant Professor, ETH Zurich, Institute of Environmental Engineering, CH- 8093 Zurich, Switzerland.

Empa, Swiss Federal Laboratories for Materials Science and Technology, CH-8600 Dübendorf, Switzerland
ETH Zurich, Institute of Environmental Engineering, CH- 8093 Zurich, Switzerland

A Centrifugal Particle Mass Analyzer and modified Differential Mobility Spectrometer were used to measure the mass and mobility of particulate matter emitted by CFM56-5B4/2P, CFM56-7B26/3 and PW4000-100 gas turbine engine sources. The mass-mobility exponent of the particulate matter from the CFM56-5B4/2P engine ranged from 2.68 to 2.82, while the effective particle densities varied from 600 to 1250 kg/m^3 depending on the static engine thrust and sampling methodology used. The effective particle densities from the CFM56-7B26/3 and PW4000-100 engines also fell within this range. The sample was conditioned with or without a catalytic stripper and with or without dilution, which caused the effective density to change, indicating the presence of condensed semi-volatile material on the particles. Variability of the determined effective densities across different engine thrusts, based on the scattering about the line of best fit, was lowest for the diluted samples and highest for the undiluted sample without a catalytic stripper. This variability indicates that the relative amount of semi-volatile material produced was engine thrust dependent. It was found that the non-volatile PM effective particle density (in kg/m^3) of the CFM56-5B4/2P engine at relative thrusts below 30% could be approximated using the particle mobility diameter (d_{me} in m) with $11.92 d_{me}^{(2.76-3)}$.

Nomenclature

d_{me} = particle mobility diameter

k = mass-mobility pre-factor

m = particle mass

n = particle number concentration

u_x = uncertainty of parameter x

C = mass-mobility scaling component

CMD = count median diameter

D_m = mass-mobility exponent

M = suspended particle mass concentration

P = DMS classifier pressure

Q_s = DMS classifier sample flow rate

Q_{sh} = DMS classifier sheath flow rate

T_c = DMS classifier temperature

ρ_{eff} = effective particle density

I. Introduction

AIRCRAFT gas turbine engine emissions can negatively impact the environment [1,2], the global climate [3–5] and human health [6,7]. These emissions are expected to grow as revenue passenger miles are predicted to increase an average of 2.2% per year domestically in the United States and 4.2% per year internationally over the next 20 years [8]. Therefore, accurate characterization is required for effective and potential future regulation.

Non-volatile particulate matter (PM) emissions at the turbine engine exhaust plane consist mainly of black carbon (BC) aggregates [9]. BC aggregates are an example of mass-fractal aggregates which are comprised of primary particles [10] where measurable features of the aggregates are related to desired properties such as the number of primary particles per aggregate or the aggregate mass using power-law relationships [11–14]. One such relationship involves the mass-mobility exponent (D_m) which relates the particle mass (m) to its mobility diameter (d_{me}) by:

$$m = C \cdot d_{me}^{D_m} \tag{1}$$

where C is a scaling constant. McMurry et al. [15] extended this theory further by defining the effective particle density (ρ_{eff}) as:

$$\rho_{eff} = \frac{6}{\pi} \cdot \frac{m}{d_{me}^3} = k \cdot d_{me}^{D_m - 3} \quad (2)$$

where k is the mass-mobility pre-factor ($k=6C/\pi$). This equation is typically fitted to mass-mobility results of aerosol samples extracted from combustion sources, such as flames [16] and diesel engines[17–19], as these particles usually exhibit fractal-like properties.

Mass-mobility relationships can be used to determine characteristics of particle morphology [20] or to calculate mass distributions from mobility size distributions [21,22]. Previous aerosol studies of gas turbine engine exhaust, based on the measurement of particle mobility size distributions, have assumed that the particles were solid spheres that have unit density [23–28] or the bulk density of carbon (1500-1900 kg/m^3) [29–31] to determine mass distributions. These assumptions are questionable as the particles are expected to be non-spherical and follow a fractal-like relationship causing the effective density to be a function of the particle size. Therefore, knowledge of the mass-mobility relationship or a known density function would avoid these assumptions and could yield more accurate results in predicting mass distributions and emissions.

Many studies have characterized aircraft exhaust in terms of PM number emission indices [32,33], PM mass emission indices [34,35], gas phase emissions [36,37] or other characteristics [38]; however, only a few studies have determined the effective PM density. Onasch et al. [39], using the relationship between particle vacuum aerodynamic diameter (measured using an Aerosol Mass Spectrometer, AMS) and mobility diameter (measured using a Scanning Mobility Particle Sizer, SMPS), reported an average effective density of the soot produced by a CFM56-2-C1 turbine engine at high throttle to be approximately 1000 kg/m^3. Li-Jones et al. [40] also inferred an average effective density of 1000 kg/m^3 from a T700-GE-700 helicopter engine at idle conditions, using gravimetric filters to determine the total particle mass and the measured size distribution to calculate the total particle volume. Timko et al. [9] determined the effective densities from a PW308 turbine engine using two different methodologies. The first method, like the previous studies, determined the average effective density using an AMS and SMPS. This value was found to be between 710 kg/m^3 to 840 kg/m^3 depending on the type of fuel used and engine thrust. The second method determined the average effective density from the total particle mass measured using a Multi-Angle

Absorption Photometer (MAAP) and the total particle volume measured using an SMPS. This value was found to range from 400 kg/m^3 to 820 kg/m^3 depending on the type of fuel used and engine thrust.

This paper describes the mass-mobility distributions of aircraft exhaust particles measured using a Centrifugal Particle Mass Analyzer (CPMA, Cambustion) and modified Differential Mobility Spectrometer (mDMS, based on a Cambustion DMS500) system. This system provides the size-resolved effective densities of PM, allowing the non-volatile particulate matter (nvPM) mass concentration to be calculated from the measured non-volatile mobility size distribution. Thus one mobility-sizing instrument, such as a SMPS or DMS, could potentially be used to measure both the number and mass concentration measurements required by proposed future regulations [41] if the mass-mobility relationship was determined for the given engine, its operating conditions and sampling parameters. Previous aircraft effective density studies, as described above, measured the mass-weighted average effective density and therefore did not account for the change in effective density with particle mobility size when calculating the nvPM mass concentration. Furthermore, this paper discusses the effects of sample dilution, a catalytic stripper (CS), engine type and thrust on the effective density functions.

II. Experimental Setup

The SAMPLE III.2 campaign was completed at the SR Technics gas turbine engine testing facility at Zürich airport, Switzerland from April 23rd to May 4th 2012. The campaign was carried out by a collaboration of international researchers and involved several simultaneous tests during aircraft engine exhaust sampling. Three days of dedicated testing of the CFM56-5B4/2P turbofan engine, where the engine test conditions were set by the researchers, were completed from April 28th to 30th 2012. The dedicated engine tests were complemented by measurements during post-maintenance runs of SR Technics customers' engines CFM56-7B26/3 and PW4000-100. The dedicated engine CFM56-5B4/2P has a dual annular combustor (DAC) designed for low NOx emissions. Non-volatile particulate matter emissions from this engine peak at around 30% of maximum thrust before the combustor staging point and with further thrust drop virtually to zero. The latter two engine models (CFM56-7B26/3 and PW4000-100) are equipped with traditional single annular combustors (SAC) where the non-volatile PM emissions increase monotonically with thrust [42]. Although the SAC engines prevail in the current fleet, the newest low emissions combustors with twin annular premixing swirlers (TAPS) have emissions characteristics very similar to the DAC engines when the certification smoke number is taken as a surrogate for the non-volatile PM [43].

A. Sampling aircraft turbine engine exhaust

The experimental set-up used to collect, condition, and transport the aircraft turbine exhaust to the measurement systems is shown in Fig. 1. A table outlining the components, materials and dimensions of the sampling system is shown in the online Supplemental Information. The sample was collected using an 8 mm ID single point probe placed downstream of the engine exhaust nozzle. The horizontal distance of the exhaust plane to the sampling head inlet was 1.055 m for the CFM56-5B4/2P, 0.695 m for the CFM56-7B26/3 and 1.735 m for the PW4000-100 engine. The probe was traversable in the vertical plane, but was maintained at a previously determined engine specific vertical location. The sampling probe temperature was kept above 160˚C using a 35 mm ID coaxial probe sleeve that forced hot exhaust flow around the 10 mm OD sampling tube of the probe. All components downstream of the probe were maintained at the shown temperatures in Fig. 1 using electrical heat tracing or heating bags to avoid the condensation of semi-volatile material or water (Table S1).

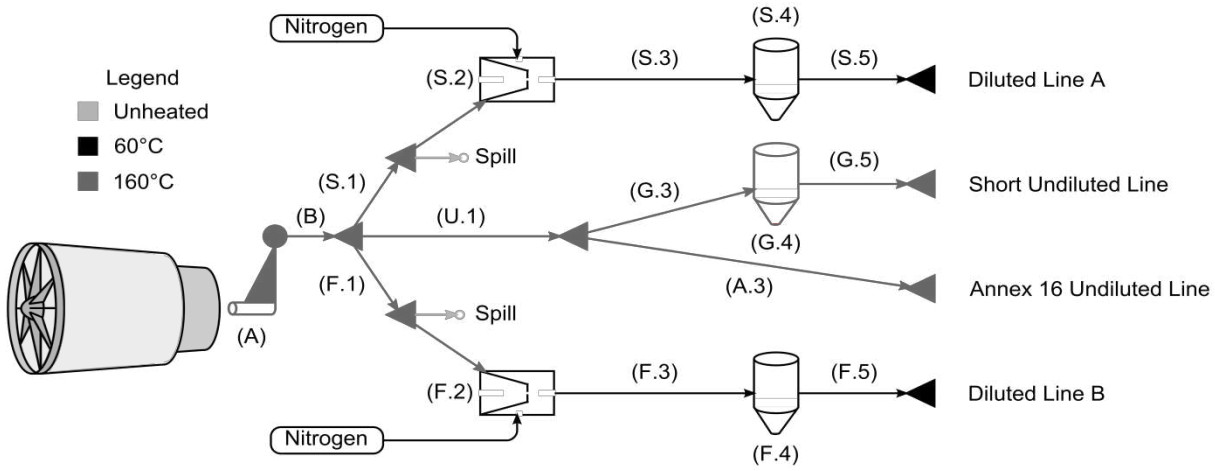

Fig. 1 Sampling system used to collect aircraft exhaust from the engine exit plane and transport it to the measurement systems. The sampling system consisted of the following components: (A) Sample Probe; (B) Primary Sample Line; (S.1) Diluted Primary Line A; (U.1) Undiluted Primary Line; (F.1) Diluted Primary Line B; (S.2) Primary Dilutor A; (F.2) Primary Dilutor B; (S.3) Diluted Sample Line A; (G.3) Short Undiluted Sample Line; (A.3) Annex 16 Undiluted Sample Line; (F.3) Diluted Sample Line B; (S.4) BGI Sharp-Cut Cyclone; (G.4) BGI Sharp-Cut Cyclone; (F.4) URG Stairmand Cyclone; (S.5) Diluted Secondary Line A; (G.5) Short Undiluted Secondary Line; (F.5) Diluted Secondary Line B.

Particles were sampled at the end of four sampling lines as shown in Fig. 1. Two sample lines were diluted relatively near the sample probe (Diluted Lines A and B) and two sample lines were undiluted (the Short Undiluted Line and the Annex 16 Undiluted Line). Diluted Lines A and B both diluted the sample with 5.0 nitrogen by a 10(±2):1 ratio using a Dekati DI-1000 eductor diluter and a nitrogen heater (DH-1723, Dekati). These diluted lines had the following differences; Diluted Line A had a 1 inch to 3/8 inch ID three-way splitter (S.1) and the main

sample line (S.3) was 25 m long with a 7.75 mm ID. Diluted Line B had an 8 mm ID three-way splitter (F.1) and the main sample line (F.3) was 24.5 m long with an 8 mm ID. These differences were assumed to have negligible impact on the sample conditioning imparted by the sampling line when generating the results for this paper. The Short Undiluted Line was used to measure the sample as close as possible to the engine exhaust nozzle, while the Annex 16 Undiluted Line was used to complete gas phase regulation measurements [44]. Both of these undiluted lines only conditioned the sample through line heating at 160°C. The total length of the Annex 16 Undiluted Line and Short Undiluted Line from the primary sample line (labelled as B in Fig. 1) outlet were 25.34 m and 1.74 m respectively (1.11 m and 24.71 m shorter than Diluted Line A respectively).

The placement of the aerosol characterization instruments on each sample line when the CPMA-mDMS system was used is shown in Fig. 2. A table outlining the characteristics of these instruments is shown in the online Supplemental Information. The CPMA-mDMS system measured the exhaust from a CFM56-5B4/2P turbine engine on April 29th and April 30th, a CFM56-7B26/3 turbine engine on May 2nd and a PW4000-100 turbine engine on May 3rd. The arrangement of the instruments changed from day to day to test the effects of different sampling parameters such as the sample line temperature and length on the results. Further details about the sampling system and the results comparing the sampling parameters are described by Crayford et al. [45].

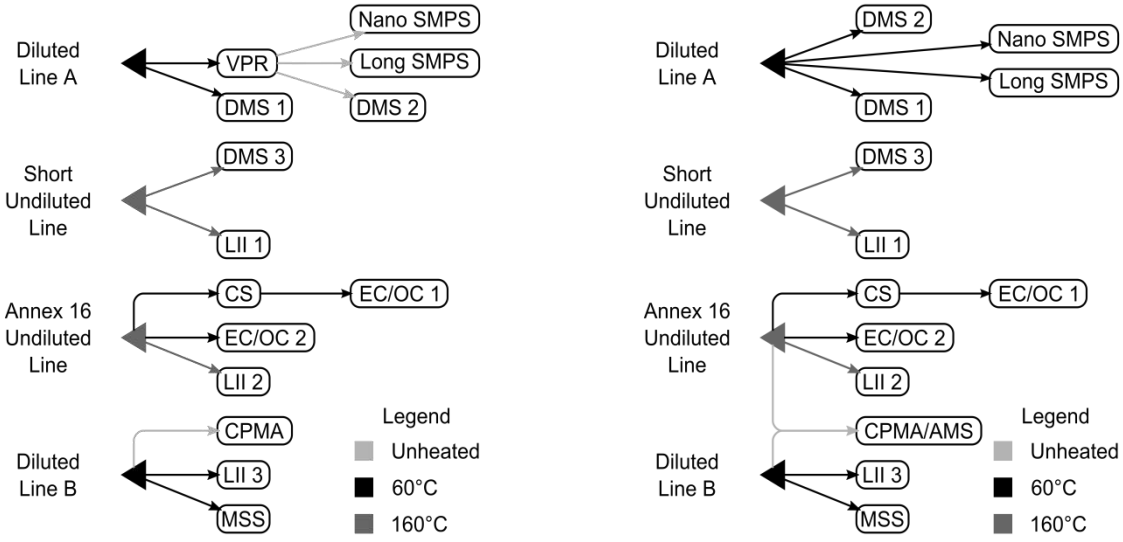

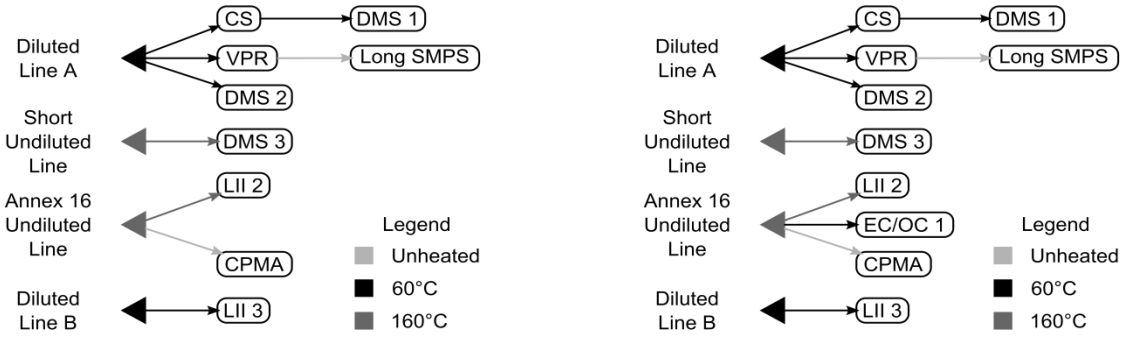

Fig. 2 Aerosol instrumentation used for: (a) CFM56-5B4/2P turbine engine on April 29th 2012; (b) CFM56-5B4/2P turbine engine on April 30th 2012; (c) CFM56-7B26/3 turbine engine on May 2rd 2012; (d) PW4000-100 turbine engine on May 3rd 2012. The arrangement of the CPMA-mDMS relative to the AMS system (Fig. 2b) is shown in Fig. 3.

B. CPMA-mDMS system

The experimental configuration of the CPMA-mDMS system is shown in Fig. 3. This set-up was used rather than a Differential Mobility Analyzer (DMA), CPMA and Condensation Particle Counter (CPC) system due to the short sampling time allowed at each engine thrust point. The DMA-CPMA-CPC system must scan the mass-space of the mobility size selected particles to determine the average particle mass, while the CPMA-DMS system can measure the real-time effective density at one mass setpoint [46]. Therefore, a CPMA-DMS system is capable of measuring an eight point effective density function in approximately the same time as a DMA-CPMA-CPC system measuring one point [46]. The higher temporal resolution of the CPMA-mDMS system results in a slightly higher effective density uncertainty (9.5%-10.4%) compared to the one of the DMA-CPMA-CPC system (9.4%) [46].

Three-way valves A and B, shown in Fig. 3, were only used on April 30th and allowed the CPMA-mDMS system to sample from either Diluted Sample Line B or the Annex 16 Undiluted Sample Line. To maintain system flow balance, the line that was not being sampled by the CPMA-mDMS system was sampled by an Aerosol Mass Spectrometer (AMS). For the other test days valves A and B were removed and the CPMA sampling locations indicated in Fig. 2 were connected directly to the inlet of three-way valve C. To test the effects of particle volatility, three-way valve C allowed the sample to bypass the catalytic stripper (CS)[47–49]. The catalytic stripper was heated to 350˚C and consisted of two ceramic substrates: an oxidation catalyst and a sulfur trap.

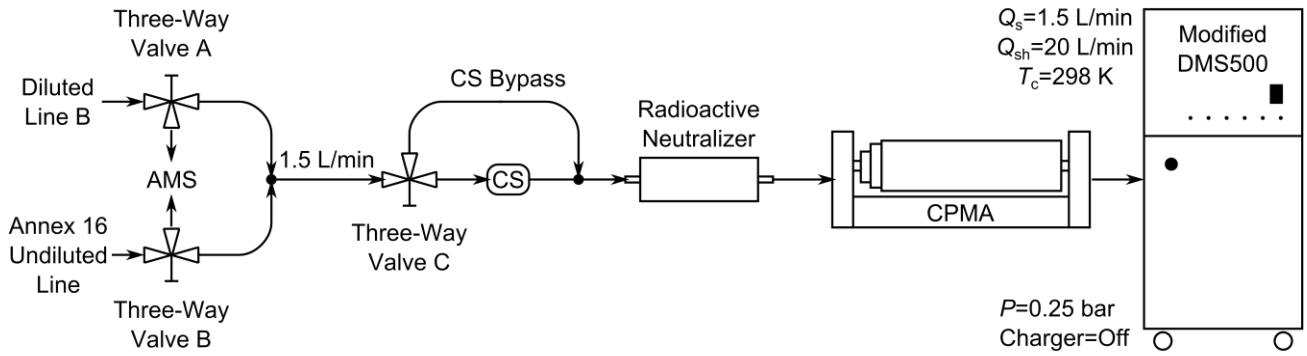

Fig. 3 Experimental set-up of the CPMA-mDMS system that was used to measure the mass-mobility of individual aerosol particles where: CS is a catalytic stripper, Q_s is the DMS classifier sample flow rate, Q_{sh} is the DMS classifier sheath flow rate, T_c is the DMS classifier temperature and P is the DMS classifier pressure.

A radioactive neutralizer was used to bring the sample upstream of the CPMA to a defined bipolar charge distribution. The CPMA classifies charged particles by their mass-to charge ratio [50]. This is accomplished by passing the sample between two concentric spinning cylinders, thus applying a centrifugal force to the particles. A voltage potential is also placed across the cylinders applying an electrostatic force to the particles as well. Therefore particles of a set mass-to-charge ratio induce an equal electrostatic and centrifugal force in opposite directions and pass through the classifier. By changing the voltage and speed applied to the cylinders, the mass-to-charge setpoint can be controlled. Uncharged particles can also pass through the CPMA if they are smaller than the cut-off mass for a given rotational speed [51].

A modified DMS500 (mDMS) was used to measure the mobility size distribution of the CPMA classified particles. The DMS500 classifies particles by their electrical mobility near real time with a 10 Hz resolution, thus measuring the transient mobility size distribution [52,53]. A voltage potential is placed between two concentric cylinders and the path of the particles from the inside cylinder to the outside cylinder is only dependent on their electrical mobility. Twenty-two electrometer rings are placed on the inner surface of the outer cylinder and measure the current generated from these particles grounding their charges at impact. By applying an inversion to these measured currents the electrical mobility size spectrum of the particles is determined.

The DMS500 unipolar charger is a significant source of uncertainty, both for particles in the range of 20-80 nm (in the region where doubly-charged particles start to occur), and due to morphological sensitivity of the charging process [54,55], compared with its classifier alone. Therefore the charger was disabled and the mDMS was run as a particle mobility classifier, relying on the pre-existing charge from the neutralized and CPMA classified aerosol, in an attempt to improve the sizing accuracy and remove most of the morphological dependence from the

measurement. As a result, the particles had lower charge states and thus lower electrical mobilities and required a longer residence time within the mDMS to be classified. This was achieved by decreasing the mDMS sheath and sample flow rates from 30 L/min to 20 L/min and 8 L/min to 1.5 L/min respectively compared to the standard DMS. These modifications limited the sizing range of the mDMS from 10 to 120 nm compared to the standard 5 to 1000 nm range. The inversion matrix applied to the mDMS assumed all particles were singly charged and generated 64 size-classes per decade compared to the standard DMS inversion which generated 16 size-classes per decade. These modifications allowed the CPMA to operate at higher resolutions at lower speeds (due to the lower sample flow through the CPMA). In addition, the mDMS measurements were not affected by small uncharged particles that passed through the CPMA, as these particles were not detected on the mDMS electrometer rings.

The mDMS measured the mobility size distribution of several different particle masses since the CPMA classified the particles by their mass-to-charge ratio and multiply-charged particles were present. Therefore the results had to be corrected for this effect. The average shift due to this multiply-charged particle correction was less than 5% in terms of effective density for all of the data herein. This correction was accomplished by measuring the aerosol size distribution independently‡‡‡‡‡, using either an SMPS or DMS. The charge distribution of the neutralized aerosol was calculated using the bipolar charging approximation equations developed by Wiedensohler [56], then the theoretical CPMA and DMS transfer functions were applied to this distribution, determining the theoretical DMS ring currents generated. The difference between the experimental and theoretical DMS ring currents was minimized using three scaling factors. After minimization the fraction of DMS ring current generated by multiply-charged particles was removed and the corrected currents were reinverted to determine the corrected DMS mobility size distribution. This distribution was fitted with a lognormal function and the fitted count median diameter (CMD) was corrected with the size calibration curve shown in the online Supplemental Information. The average shift due to this size calibration was less than 7% in terms of effective density for all of the data herein. By combining the multiply-charge corrected and size calibrated CMD and the CPMA mass-to-charge setpoint the average effective density of that setpoint was determined. Further details of the CPMA-mDMS setup, the multiple-charge correction process and its experimental validation are described by Johnson et al. [46]. The uncertainty of the CPMA-mDMS system was 3.0-3.4% in terms of mobility size and 9.5-10.4% in terms of effective density

‡‡‡‡‡ For some cases the unclassified mobility size distribution was approximated from a distribution measured on a different sample line by accounting for the different dilution ratios measured using gas analyzers and using a model developed by Liscinsky and Hollick [67] to approximate the differences in the particle losses between the two lines.

depending on the particle mobility size [46]. These uncertainties apply to all of the effective density results shown in this paper.

III. Results and discussion

The effective particle densities measured from the CFM56-5B4/2P turbine engine on April 29th and 30th at each engine thrust point are shown in Fig. 4. Typical of combustion sources, the effective particle density decreased as mobility size increased indicating the particles were fractal-like aggregates. Therefore the experimental data were fitted with the mass-mobility relationship for a fractal-like particle, as defined by Equation (2), using chi-squared minimization. The quality of the fit was determined by the standard error of fit as defined by Figliola and Beasley [57], which measures the deviation of the data from the line of best fit.

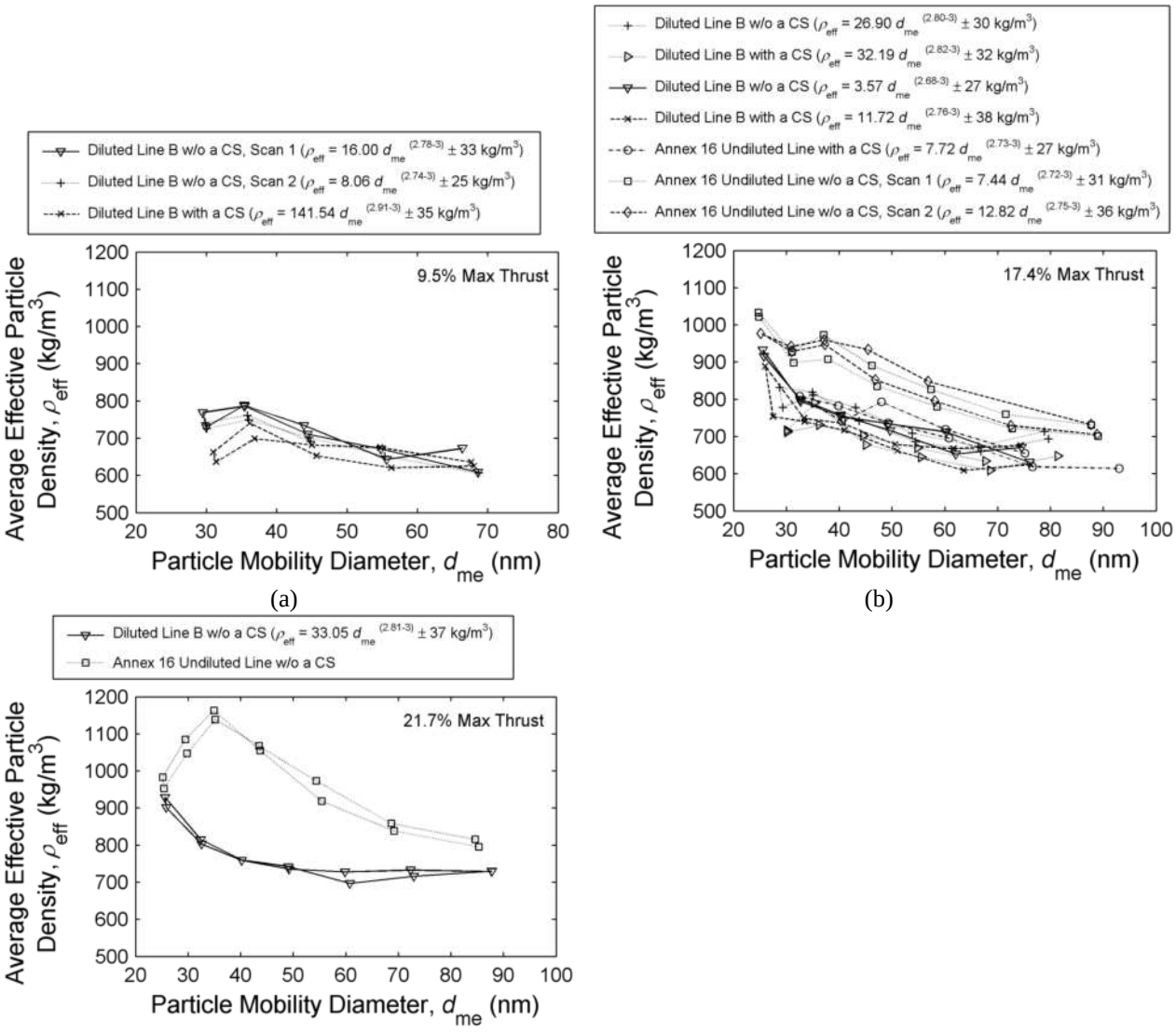

(c)

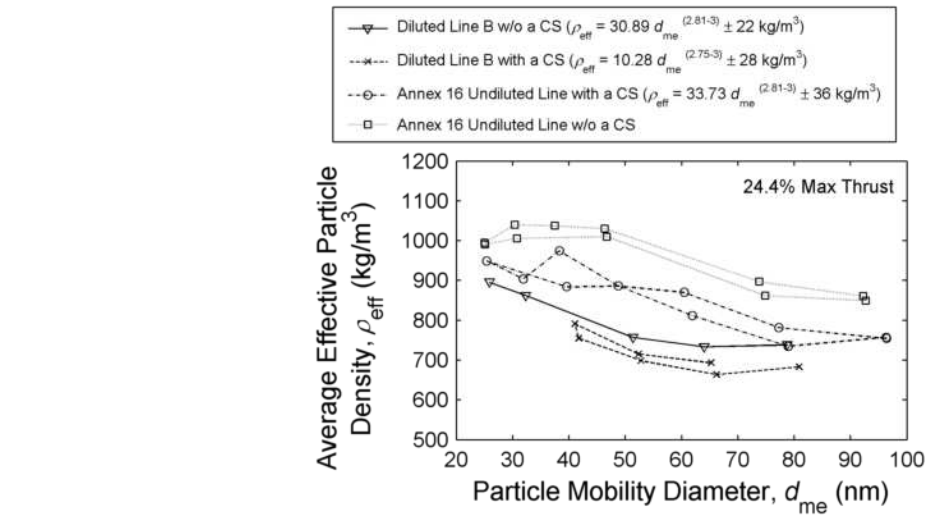

(d)

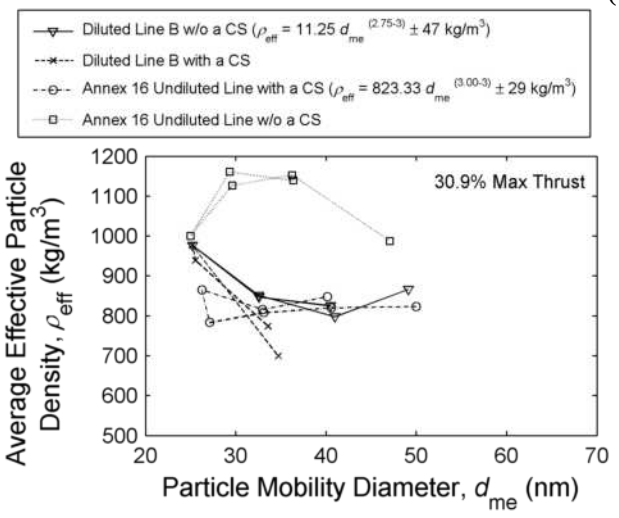

(e)

Fig. 4 Effective particle density results from CFM56-5B4/2P turbine engine at (a) 9.5%; (b) 17.4%; (c) 21.7%; (d) 24.4%; (e) 30.9% maximum thrust (measured ambient test cell corrected static thrust).

Effective density functions that did not follow a fractal-like relationship were not fitted. This case occurred where a maximum effective density appeared in the middle of the effective density function as shown in the Annex 16 Undiluted Line without a CS data in Fig. 4c, Fig. 4d and Fig. 4e. One possible explanation for this peak is the CPMA classified an externally mixed, or multiple species, sample of varying effective densities. The undiluted line without a CS had the highest possibility of delivering a multi-species sample. Furthermore, the CPMA-mDMS system did not have the resolution to resolve these different modes. The CPMA was operated using a lower resolution of 3 or a normalized transfer function full width at half maximum of 1/3 to ensure the mDMS had adequate signal. Therefore, the CPMA-mDMS system determined the average effective particle density of the mixture, which could be dominated by one mode or another depending on the CPMA setpoint, thus generating the

effective density peak. Narrow effective density functions were also not fitted with the mass-mobility relationship, as shown in Fig. 4e Diluted Line B with a CS. This effective density function only consisted of a few data points, due to insufficient mDMS signal from low particle concentrations, and therefore did not accurately represent the mass-mobility relationship over the entire particle mobility size distribution.

The mass-mobility exponent varied between 2.68 and 2.82 for all CFM56-5B4/2P engine thrusts and different sample conditioning. A few mass-mobility exponents did fall outside this range. Fig. 4a Diluted Line B with a CS depicts a mass-mobility exponent of 2.91. This high value was caused by the data points with the two smallest mobility sizes having lower effective particle densities than the rest of the function. If these data points are considered outliers the remaining effective density function followed a fractal-like relationship. A mass-mobility exponent of 3.00 is also shown in Fig. 4e Annex 16 Undiluted Line with a CS. The effective particle densities for this engine thrust point and sample conditioning were approximately constant. The exact particle compositions of this particular mass-mobility relationship are still unknown and require further investigation.

The mass-mobility pre-factor was found to be highly sensitive to the mass-mobility exponent. Disregarding the two outlier cases, the mass-mobility exponent varied by a maximum of 2.9% of its average value, while the mass-mobility pre-factor varied by an order of magnitude, 3.57 to 33.73. The mass-mobility pre-factor increased exponentially as the mass-mobility exponent decreased. Due to this dependency the change in effective density was essentially described by the change in the mass-mobility exponent alone.

At the same particle mobility sizes across all engine thrust points with the sample passing through the CS, Diluted Line B had on average a 76.8 kg/m^3 lower effective density than the Annex 16 Undiluted Line. If the sample bypassed the CS, Diluted Line B had on average a 170 kg/m^3 lower effective density than the Annex 16 Undiluted Line. Similarly, sample that passed through the CS had on average a 44.4 kg/m^3 lower effective density than the sample that bypassed the CS from Diluted Line B and a 156 kg/m^3 lower effective density from the Annex 16 Undiluted Line. These shifts in the effective density functions indicate the presence of semi-volatile material within the sample. As expected the shift with and without a CS was smaller in the diluted line than the undiluted line, as the dilution lowered the semi-volatile material partial vapor pressure in the line, making it less likely for semi-volatile material to condense. The presence of semi-volatile material in aircraft exhaust has been observed in other studies, such as Anderson et al. [58] and Peck et al. [28]. Therefore, for the conditions described above sufficient sample

dilution and to a smaller extent a volatile component remover, such a catalytic stripper, volatile particle remover (VPR) or thermodenuder, should be used to characterize the non-volatile particulate matter.

Semi-volatile material usually has a lower bulk density than non-volatile material (assumed to be black carbon), approximately 900 kg/m^3 vs. 1800 kg/m^3 [59] respectively. Nonetheless, as the fraction of semi-volatile material increases the effective particle density will also increase due to the branched-aggregate nature of a soot particle, where the semi-volatile material fills in the voids around the primary soot particles, thus increasing the particle mass significantly, while only causing a small increase in the particle mobility diameter. This theory is supported by the values above as the measured effective density, at the same mobility size, increased under conditions where more semi-volatile material was likely present.

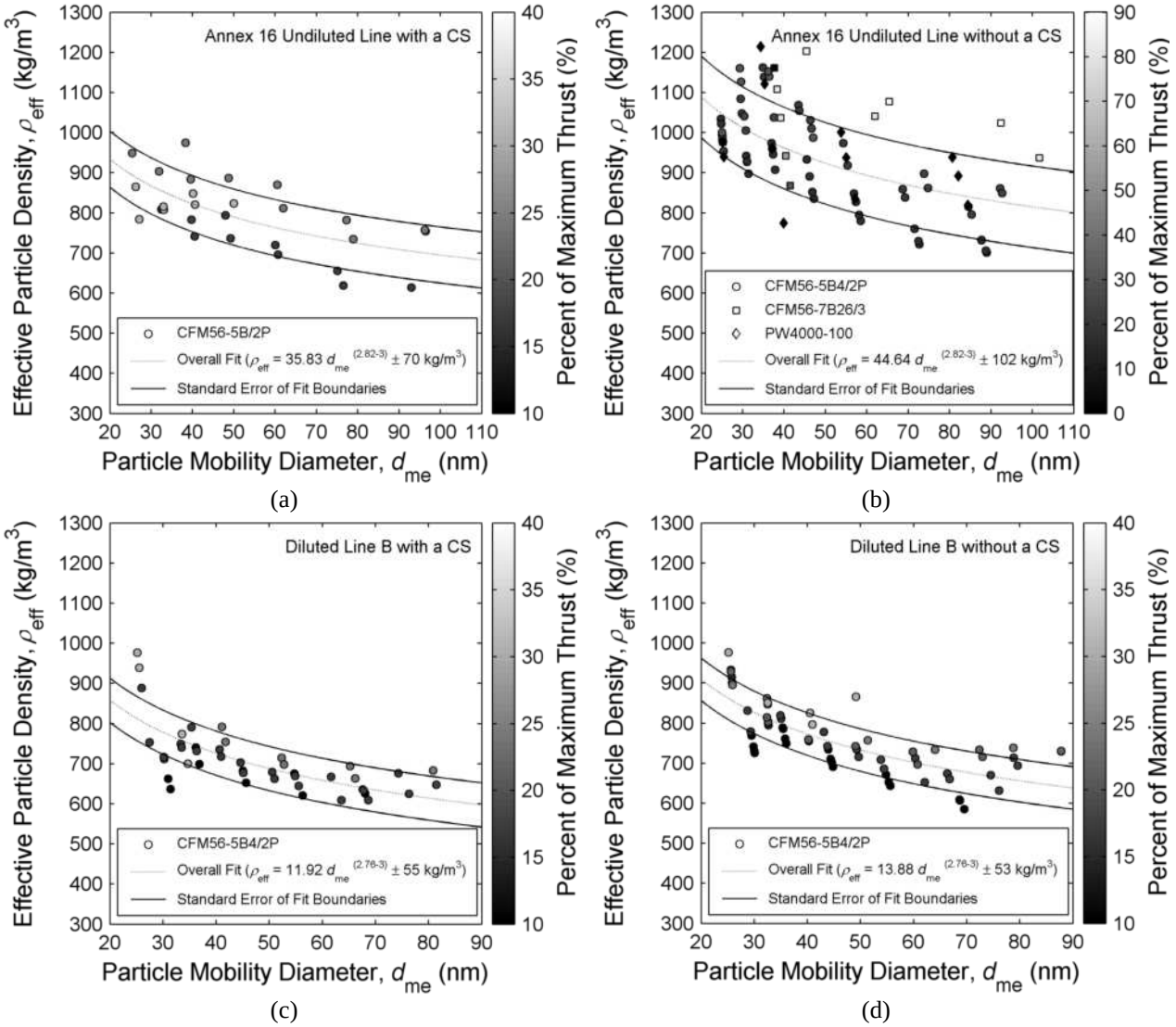

Fig. 5 Effective density functions for different engines at different thrust levels, where the solid lines indicate the limits of the standard error of fit, measured from: (a) Annex 16 Undiluted Line with a CS; (b) Annex 16 Undiluted Line without a CS; (c) Diluted Line B with a CS; (d) Diluted Line B without a CS.

The variations in effective density functions due to engine thrust for each sample conditioning are shown in Fig. 5. The color of each data point corresponds to the engine thrust level. Many of the cases show that the effective particle density increased as engine thrust increased. However, Fig. 5a illustrates another trend that the effective density initially increased as engine thrust increased, then decreased for higher engine thrust. Timko et al. [9] found that the average effective density, measured using an AMS and SMPS, increased slightly as engine thrust increased. However using a MAAP and SMPS, which measures a different definition of effective density than the AMS and SMPS, Timko et al. [9] found that this average effective density initially increased as engine thrust increased then decreased at higher engine thrust. The CPMA-mDMS results can be compared against Timko's second measurement of effective density as both methods are based on particle mass and mobility diameter. Using the MAAP and SMPS, Timko et al. [9] measured a mass-weighted average effective density of 400 kg/m^3 to 820 kg/m^3, which falls within the range of the size-resolved effective densities measured by the CPMA-mDMS system of approximately 600 kg/m^3 to 1250 kg/m^3.

To determine the change in effective density due to engine thrust, yet account for the effective density being a function of particle mobility size, the standard error of fit was determined for each sampling condition. With and without the CS the samples from Diluted Line B had standard errors of fit of 55 kg/m^3 and 53 kg/m^3 respectively, while with and without the CS the samples from the Annex 16 Undiluted Line had standard errors of fit of 70 kg/m^3 and 102 kg/m^3 respectively. Therefore, engine thrust had the smallest effect on the diluted line (Fig. 5c and Fig. 5d) and the largest effect on the undiluted line without a CS (Fig. 5b) as depicted by the spread of the effective density in each plot at common mobility sizes. These trends indicate greater variability of effective particle density for the undiluted lines and that this is likely linked to the different partitioning of the semi-volatile content in the two lines.

Fig. 5b also shows the effective densities from three different turbine engines: CFM56-5B4/2P, CFM56-7B26/3 and PW4000-100. At low thrust, the effective densities of PM produced by these two other engines were similar to the CFM56-5B4/2P engine results.

Fig. 6 shows all of the results from the diluted line with a CS or the nvPM effective densities measured across all of the CFM56-5B4/2P engine thrust points. The shaded region shown in Fig. 6 outlines the standard error of the mass-mobility fit, as described previously, and was determined to be ±55 kg/m^3. Therefore, due to the small

variation in nvPM effective density from engine thrust, the nvPM effective density function for the CFM56-5B4/2P engine at relative thrust levels below 30% can be approximated by:

$$\rho_{\mathrm{eff}} = 11.92 \cdot d_{\mathrm{me}}^{2.76-3} \pm 55 \tag{3}$$

where d_{me} is in m and ρ_{eff} is in kg/m^3.

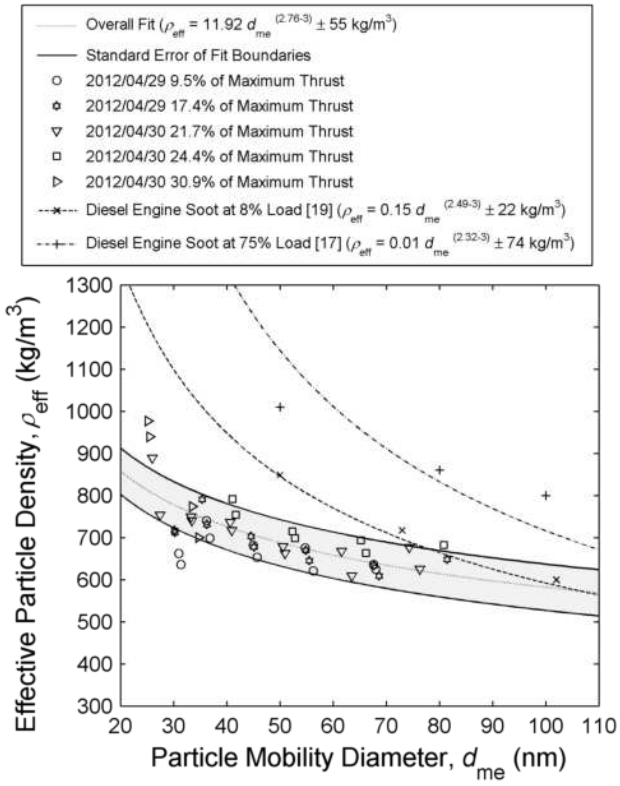

Fig. 6 Average non-volatile effective particle density, measured on Diluted Line B with a CS, from a CFM56-5B4/2P turbine engine across all measured thrust points and compared against previous studies of diesel engine soot.

For comparison Fig. 6 also shows effective density data (and fits of the data) from two diesel engines [17,19] at operating conditions that produce little volatile material, and thus, should be comparable to the non-volatile effective density of the turbine soot. The mass-mobility exponent of 2.76 for the turbine soot is higher than previously measured values from PM produced by a diesel engine. Park et al. [18] measured a diesel engine mass-mobility exponent of 2.32, while Olfert et al. [19], at low diesel engine load points, measured mass-mobility exponents of 2.22 to 2.48. A typical mass-mobility exponent for fractal aggregates is approximately 2.2 [14], however Ghazi et al. [60] have shown that the mass-mobility exponent can be higher if the primary particle size increases with the aggregate mobility size. Transmission electron microscopy images collected during the SAMPLEIII.2 campaign have shown that the primary particle size of aircraft turbine engine PM does increase with the project-area

equivalent diameter [61], which is directly proportional to the particle mobility diameter [62]. This effect could explain why the mass-mobility exponent of aircraft turbine engine PM is higher than diesel engine PM. Furthermore, the effective density of the aircraft PM tends to be lower than the diesel PM. As shown by Eggersdorfer et al. [63], a smaller primary particle size will result in a lower effective density for a given aggregate mobility. The primary particle size of the aircraft turbine engine PM (~10 to 30 nm for the aggregate sizes measured here [59]) is generally smaller than typical diesel engine PM (20-40 nm [18]).

The measured effective density functions can be used to calculate the suspended particle mass distribution if the particle mobility size-distribution is known or measured using a DMS or SMPS, for example. Previous studies with diesel engine soot have shown that the DMS is capable of measuring mass concentrations with a known density function [64]. These measurements are expected to be within 37.5% of the true value for a 95% confidence interval, determined by propagating the DMS particle mobility sizing uncertainty of 10% [55] and DMS particle number counting uncertainty without dilution of 20% [55] with the CPMA-mDMS system upper limit effective density uncertainty of 10.4% [46].[§§§§§] Similarly, an SMPS is expected to measure the suspended particle mass concentration within 17.0% of the true value for a 95% confidence interval. This was determined by propagating the CPC counting uncertainty of 10% [65] with the DMA particle mobility size uncertainty of 3% [66] and the CPMA-mDMS system upper limit effective density uncertainty of 10.4% [46].

IV. Conclusion

A CPMA-mDMS system was used to measure the size-resolved effective density of aircraft particle matter. The mass-mobility exponent was found to be between 2.68 and 2.82 for varying CFM56-5B4/2P engine thrust points, with only two exceptions. Effective density functions that displayed a peak in the middle were not fitted with the mass-mobility relationship. This peak was thought to be caused by the CPMA classifying multiple species of varying particle effective densities. The shift in effective density with and without a CS of 44.4 kg/m^3 on the diluted

[§§§§§] The particle mass concentration (M) can be determined from: $M = \sum_{i=1}^{N} \frac{\pi}{6} n_i \cdot \rho_{\text{eff}_i} \cdot d_{\text{me}_i}^3$, where n_i is the particle number concentration for each particle mobility size bin. Since the uncertainties are approximately constant across all of the size bins, the particle mass concentration uncertainty, neglecting any uncertainty from the data inversion process in the sizing instruments, can be determined from:

$\frac{u_M}{M} = \sqrt{\left(\frac{u_n}{n}\right)^2 + \left(\frac{u_{\rho_{\text{eff}}}}{\rho_{\text{eff}}}\right)^2 + 9 \cdot \left(\frac{u_{d_{\text{me}}}}{d_{\text{me}}}\right)^2}$, where u is the uncertainty.

line and 156 kg/m^3 on the undiluted line indicates the presence of condensed semi-volatile material. At low thrust points, the effective particle densities from CFM56-7B26/3 and PW4000-100 engines were similar to the CFM56-5B4/2P engine. The change in effective density due to engine thrust was found to be the smallest on the diluted line and largest on the undiluted line. This variability in effective particle density could be caused by higher semi-volatile content aerosol in the undiluted samples. The overall small deviation in the nvPM effective density from the CFM56-5B4/2P engine at low thrust allowed it be approximated using a mass-mobility pre-factor of 11.92 and exponent of 2.76, with a standard error of fit of 55 kg/m^3.

Acknowledgments

This research would not have been possible without the financial support of the European Aviation Safety Agency (EASA) Contract No: EASA.2010.FC10 Specific Contract Sample III - SC02 and the Swiss Federal Office of Civil Aviation (FOCA) project "Particulate Matter and Gas Phase Emission Measurement of Aircraft Engine Exhaust". The contributions of Cambustion, Green Aviation Research and Development Network (GARDN), MDS Aero Support Corporation, Natural Sciences and Engineering Research Council of Canada (NSERC) and Alberta Innovates-Technology Futures were also significant to this research. Special thanks go to Frithjof Siegerist and his team at SR Technics for engine operation and test cell facility access. BB thanks the financial support of Swiss Federal Laboratories for Materials Science and Technology EMPA postdoc fellowship.

References

[1] Unal, A., Hu, Y. T., Chang, M. E., Odman, M. T., and Russell, A. G., "Airport related emissions and impacts on air quality: Application to the Atlanta International Airport," *Atmospheric Environment*, vol. 39, 2005, pp. 5787–5798.

[2] Woody, M., Baek, B. H., Adelman, Z., Omary, M., Lam, Y. F., West, J. J., and Arunachalam, S., "An assessment of Aviation's contribution to current and future fine particulate matter in the United States," *Atmospheric Environment*, vol. 45, 2011, pp. 3424–3433.

[3] Brasseur, G. P., Cox, R. A., Hauglustaine, D., Isaksen, I., Lelieveld, J., Lister, D. H., Sausen, R., Schumann, U., Wahner, A., and Wiesen, P., "European scientific assessment of the atmospheric effects of aircraft emissions," *Atmospheric Environment*, vol. 32, 1998, pp. 2329–2418.

[4] Lee, D. S., Fahey, D. W., Forster, P. M., Newton, P. J., Wit, R. C. N., Lim, L. L., Owen, B., and Sausen, R., "Aviation and global climate change in the 21st century," *Atmospheric Environment*, vol. 43, 2009, pp. 3520–3537.

[5] Bond, T. C., Doherty, S. J., Fahey, D. W., Forster, P. M., Berntsen, T., DeAngelo, B. J., Flanner, M. G., Ghan, S., Karcher, B., Koch, D., Kinne, S., Kondo, Y., Quinn, P. K., Sarofim, M. C., Schultz, M. G., Schulz, M., Venkataraman, C., Zhang, H., Zhang, S., Bellouin, N., Guttikunda, S. K., Hopke, P. K., Jacobson, M. Z., Kaiser, J. W., Klimont, Z., Lohmann, U., Schwarz, J. P., Shindell, D., Storelvmo, T., Warren, S. G., and Zender, C. S., "Bounding the role of black carbon in the climate system: A scientific assessment," *Journal of Geophysical Research: Atmospheres*, vol. 118, 2013, pp. 5380–5552.

[6] Pope, C. A., "Review: Epidemiological Basis for Particulate Air Pollution Health Standards," *Aerosol Science and Technology*, vol. 32, 2000, pp. 4–14.

[7] Ratliff, G., Sequeira, C., Waitz, I., Ohsfeldt, M., Thrasher, T., Graham, M., and Thompson, T., *Aircraft Impacts on Local and Regional Air Quality in the United States*, 2009.

[8] FAA, "Fact Sheet - FAA Forecast for Fiscal Years 2013-2033," Mar. 2013.

[9] Timko, M. T., Yu, Z., Onasch, T. B., Wong, H.-W., Miake-Lye, R. C., Beyersdorf, A. J., Anderson, B. E., Thornhill, K. L., Winstead, E. L., Corporan, E., Dewitt, M. J., Klingshirn, C. D., Wey, C., Tacina, K., Liscinsky, D. S., Howard, R., and Bhargava, A., "Particulate emissions of gas turbine engine combustion of a fischer-tropsch synthetic fuel," *Energy and Fuels*, vol. 24, 2010, pp. 5883–5896.

[10] Dobbins, R. A., and Megaridis, C. M., "Morphology of flame-generated soot as determined by thermophoretic sampling.," *Langmuir*, vol. 3, 1987, pp. 254–259.

[11] Schmidt-Ott, A., Baltensperger, U., Gaeggeler, H. W., and Jost, D. T., "Scaling behaviour of physical parameters describing agglomerates," *Journal of Aerosol Science*, vol. 21, 1990, pp. 711–717.

[12] Koylu, U. O., and Faeth, G. M., "Structure of overfire soot in buoyant turbulent diffusion flames at long residence times," *Combustion and Flame*, vol. 89, 1992, pp. 140–156.

[13] Faeth, G. M., and Koylu, U. O., "Soot morphology and optical properties in nonpremixed turbulent flame environments," *Combustion Science and Technology*, vol. 108, 1995, pp. 207–229.

[14] Sorensen, C. M., "The mobility of fractal aggregates: A review," *Aerosol Science and Technology*, vol. 45, 2011, pp. 755–769.

[15] McMurry, P. H., Wang, X., Park, K., and Ehara, K., "The relationship between mass and mobility for atmospheric particles: A new technique for measuring particle density," *Aerosol Science and Technology*, vol. 36, 2002, pp. 227–238.

[16] Maricq, M. M., and Xu, N., "The effective density and fractal dimension of soot particles from premixed flames and motor vehicle exhaust," *Journal of Aerosol Science*, vol. 35, 2004, pp. 1251–1274.

[17] Park, K., Cao, F., Kittelson, D. B., and McMurry, P. H., "Relationship between Particle Mass and Mobility for Diesel Exhaust Particles," *Environmental Science & Technology*, vol. 37, 2003, pp. 577–583.

[18] Park, K., Kittelson, D. B., and McMurry, P. H., "Structural properties of diesel exhaust particles measured by Transmission Electron Microscopy (TEM): Relationships to particle mass and mobility," *Aerosol Science and Technology*, vol. 38, 2004, pp. 881–889.

[19] Olfert, J. S., Symonds, J. P. R., and Collings, N., "The effective density and fractal dimension of particles emitted from a light-duty diesel vehicle with a diesel oxidation catalyst," *Journal of Aerosol Science*, vol. 38, 2007, pp. 69–82.

[20] DeCarlo, P. F., Slowik, J. G., Worsnop, D. R., Davidovits, P., and Jimenez, J. L., "Particle morphology and density characterization by combined mobility and aerodynamic diameter measurements. Part 1: Theory," *Aerosol Science and Technology*, vol. 38, 2004, pp. 1185–1205.

[21] Park, K., Kittelson, D. B., and McMurry, P. H., "A closure study of aerosol mass concentration measurements: comparison of values obtained with filters and by direct measurements of mass distributions," *Atmospheric Environment*, vol. 37, 2003, pp. 1223–1230.

[22] Liu, Z., Swanson, J., Kittelson, D. B., and Pui, D. Y. H., "Comparison of Methods for Online Measurement of Diesel Particulate Matter," *Environmental Science & Technology*, vol. 46, 2012, pp. 6127–6133.

[23] Anderson, B. E., Branham, H. S., Hudgins, C. H., Plant, J. V, Ballenthin, J. O., Miller, T. M., Viggiano, A. A., Blake, D. R., Boudries, H., Canagaratna, M., Miake-Lye, R., Onasch, T. B., Wormhoudt, J., Worsnop, D. R., Brunke, K. E., Culler, S., Penko, P., Sanders, T., Han, H. S., Lee, P., Pui, D. Y. H., Thornhill, K. L., and Winstead, E., *Experiment to Characterize Aircraft Volatile Aerosol and Trace-Species Emissions (EXCAVATE)*, 2005.

[24] Wey, C. C., Anderson, B. E., Wey, C., Miake-Lye, R. C., Whitefield, P., and Howard, R., "Overview on the aircraft particle emissions experiment," *Journal of Propulsion and Power*, vol. 23, 2007, pp. 898–904.

[25] Kinsey, J. S., *Characterization of Emissions from Commercial Aircraft Engines during the Aircraft Particle Emissions eXperiment (APEX) 1 to 3*, 2009.

[26] Mazaheri, M., Johnson, G. R., and Morawska, L., "Particle and Gaseous Emissions from Commercial Aircraft at Each Stage of the Landing and Takeoff Cycle," *Environmental Science & Technology*, vol. 43, 2009, pp. 441–446.

[27] Kinsey, J. S., Timko, M. T., Herndon, S. C., Wood, E. C., Yu, Z., Miake-Lye, R. C., Lobo, P., Whitefield, P., Hagen, D., Wey, C., Anderson, B. E., Beyersdorf, A. J., Hudgins, C. H., Thornhill, K. L., Edward, W., Howard, R., Bulzan, D. I., Tacina, K. B., and Knighton, W. B., "Determination of the emissions from an aircraft auxiliary power unit (APU) during the alternative aviation fuel experiment (AAFEX)," *Journal of the Air and Waste Management Association*, vol. 62, 2012, pp. 420–430.

[28] Peck, J., Timko, M. T., Yu, Z., Wong, H.-W., Herndon, S. C., Yelvington, P. E., Miake-Lye, R. C., Wey, C., Winstead, E. L., Ziemba, L. D., and Anderson, B. E., "Measurement of volatile particulate matter emissions from aircraft engines using a simulated plume aging system," *Journal of Engineering for Gas Turbines and Power*, vol. 134, 2012.

[29] Hagen, D., Whitefield, P., Paladino, J., Trueblood, M., and Lilenfeld, H., "Particulate sizing and emission indices for a jet engine exhaust sampled at cruise," *Geophysical Research Letters*, vol. 25, 1998, pp. 1681–1684.

[30] Lukachko, S. P., Waitz, I. A., Miake-Lye, R. C., and Brown, R. C., "Engine design and operational impacts on particulate matter precursor emissions," *Proceedings of the ASME Turbo Expo*, 2005, pp. 767–785.

[31] Brundish, K. D., Clague, A. R., Wilson, C. W., Miake-Lye, R. C., Brown, R. C., Wormhoudt, J., Lukachko, S. P., Chobot, A. T., Yam, C. K., Waitz, I. A., Hagen, D. E., Schmid, O., and Whitefield, P. D., "Evolution of Carbonaceous aerosol and aerosol precursor emissions through a jet engine," *Journal of Propulsion and Power*, vol. 23, 2007, pp. 959–970.

[32] Anderson, B. E., Cofer, W. R., Bagwell, D. R., Barrick, J. W., Hudgins, C. H., and Brunke, K. E., "Airborne observations of aircraft aerosol emissions I: Total nonvolatile particle emission indices," *Geophysical Research Letters*, vol. 25, 1998, pp. 1689–1692.

[33] Corporan, E., DeWitt, M. J., Belovich, V., Pawlik, R., Lynch, A. C., Gord, J. R., and Meyer, T. R., "Emissions characteristics of a turbine engine and research combustor burning a Fischer-Tropsch jet fuel," *Energy & Fuels*, vol. 21, 2007, pp. 2615–2626.

[34] Rogers, F., Arnott, P., Zielinska, B., Sagebiel, J., Kelly, K. E., Wagner, D., Lighty, J. S., and Sarofim, A. F., "Real-time measurements of jet aircraft engine exhaust," *Journal of the Air & Waste Management Association*, vol. 55, 2005, pp. 583–593.

[35] Cheng, M.-D., Corporan, E., DeWitt, M. J., Spicer, C. W., Holdren, M. W., Cowen, K. A., Laskin, A., Harris, D. B., Shores, R. C., Kagann, R., and Hashmonay, R., "Emissions of military cargo aircraft: Description of a joint field measurement strategic environmental research and development program," *Journal of the Air & Waste Management Association*, vol. 58, 2008, pp. 787–796.

[36] Herndon, S. C., Jayne, J. T., Lobo, P., Onasch, T. B., Fleming, G., Hagen, D. E., Whitefield, P. D., and Miake-Lye, R. C., "Commercial aircraft engine emissions characterization of in-use aircraft at Hartsfield-Jackson Atlanta International Airport," *Environmental Science & Technology*, vol. 42, 2008, pp. 1877–1883.

[37] Spicer, C. W., Holdren, M. W., Cowen, K. A., Joseph, D. W., Satola, J., Goodwin, B., Mayfield, H., Laskin, A., Lizabeth Alexander, M., Ortega, J. V, Newburn, M., Kagann, R., and Hashmonay, R., "Rapid measurement of emissions from military aircraft turbine engines by downstream extractive sampling of aircraft on the ground: Results for C-130 and F-15 aircraft," *Atmospheric Environment*, vol. 43, 2009, pp. 2612–2622.

[38] Wayson, R. L., Fleming, G. G., and Kim, B., *A Review of Literature on Particulate Matter Emissions from Aircraft*, 2002.

[39] Onasch, T. B., Jayne, J. T., Herndon, S., Worsnop, D. R., Miake-Lye, R. C., Mortimer, I. P., and Anderson, B. E., "Chemical Properties of Aircraft Engine Particulate Exhaust Emissions," *Journal of Propulsion and Power*, vol. 25, 2009, pp. 1121–1137.

[40] Li-Jones, X., Penko, P. F., Williams, S., and Moses, C., "Gaseous and particle emissions in the exhaust of a T700 helicopter engine," *Proceedings of the Asme Turbo Expo*, vol. 2, 2007, pp. 395–411.

[41] SAE, "Aircraft exhaust nonvolatile particle matter measurement method development," 2010.

[42] Chang, C. T., *Low-Emissions Combustors Development and Testing*, Cleveland, Ohio, United States, February 28 - March 1, 2012: Propulsion Controls and Diagnostics (PCD) Workshop, 2012.

[43] ICAO, "ICAO Engine Exhaust Emissions Data Bank: Subsonic Engines, GEnx-2B67," Apr. 2013.

[44] ICAO, "International Standards and Recommended Practices, Environmental Protection. Annex 16 to the Convention on International Civil Aviation, Volume II, Aircraft Engine Emissions," 2008.

[45] Crayford, A., Johnson, M., Marsh, R., Sevcenco, Y., Walters, D., Williams, P., Petzold, A., Bowen, P., Wang, J., and Lister, D., *SAMPLE III: Contribution to aircraft engine PM certification requirement and standard Second Specific Contract- Final Report*, 2012.

[46] Johnson, T. J., Symonds, J. P. R., and Olfert, J. S., "Mass-Mobility Measurements Using a Centrifugal Particle Mass Analyzer and Differential Mobility Spectrometer," *Aerosol Science and Technology*, vol. 47, 2013, pp. 1215–1225.

[47] Abdul-Khalek, I. S., and Kittelson, D. B., "Real Time Measurement of Volatile and Solid Exhaust Particles Using a Catalytic Stripper," 1995.

[48] Swanson, J., and Kittelson, D., "Evaluation of thermal denuder and catalytic stripper methods for solid particle measurements," *Journal of Aerosol Science*, vol. 41, 2010, pp. 1113–1122.

[49] Swanson, J., Kittelson, D., Giechaskiel, B., Bergmann, A., and Twigg, M., "A Miniature Catalytic Stripper for Particles Less Than 23 Nanometers," *SAE Int. J. Fuels Lubr.*, vol. 6, 2013, pp. 542–551.

[50] Olfert, J. S., and Collings, N., "New method for particle mass classification - the Couette centrifugal particle mass analyzer," *Journal of Aerosol Science*, vol. 36, 2005, pp. 1338–1352.

[51] Symonds, J. P. R., Reavell, K. S. J., and Olfert, J. S., "The CPMA-Electrometer System- A Suspended Particle Mass Concentration Standard," *Aerosol Science and Technology*, vol. 47, 2013, pp. i–iv.

[52] Reavell, K., Hands, T., and Collings, N., *A Fast Response Particulate Spectrometer for Combustion Aerosols*, SAE International, 2002.

[53] Biskos, G., Reavell, K., and Collings, N., "Description and theoretical analysis of a differential mobility spectrometer," *Aerosol Science and Technology*, vol. 39, 2005, pp. 527–541.

[54] Symonds, J. P. R., and Reavell, K., *Calibration of a Differential Mobility Spectrometer*, Salzburg, Austria, September 9-14, 2007: European Aerosol Conference, 2007.

[55] Symonds, J. P. R., *Calibration of fast response differential mobility spectrometers*, National Physical Laboratory (NPL), London, UK, June 8-9, 2010: Metrology of Airborne Nanoparticles, Standardisation and Applications (MANSA), 2010.

[56] Wiedensohler, A., "An approximation of the bipolar charge distribution for particles in the submicron size range," *Journal of Aerosol Science*, vol. 19, 1988, pp. 387–389.

[57] Figliola, R. S., and Beasley, D. E., *Theory and Design for Mechanical Measurements*, John Wiley & Sons, Inc., 2010.

[58] Anderson, B. E., Cofer, W. R., Barrick, J. D., Bagwell, D. R., and Hudgins, C. H., "Airborne observations of aircraft aerosol emissions II: factors controlling volatile particle production," *Geophysical Research Letters*, vol. 25, 1998, pp. 1693–1696.

[59] Park, K., Kittelson, D., Zachariah, M., and McMurry, P., "Measurement of Inherent Material Density of Nanoparticle Agglomerates," *Journal of Nanoparticle Research*, vol. 6, 2004, pp. 267–272.

[60] Ghazi, R., Tjong, H., Soewono, A., Rogak, S. N., and Olfert, J. S., "Mass, Mobility, Volatility, and Morphology of Soot Particles Generated by a McKenna and Inverted Burner," *Aerosol Science and Technology*, vol. 47, 2013, pp. 395–405.

[61] Dastanpour, R., and Rogak, S. N., "Observations of a Correlation between Primary Particle and Aggregate Size for Soot Particles," *Aerosol Science and Technology*, [Accepted], 2014.

[62] Rogak, S. N., Flagan, R. C., and Nguyen, H. V, "The Mobility and Structure of Aerosol Agglomerates," *Aerosol Science and Technology*, vol. 18, 1993, pp. 25–47.

[63] Eggersdorfer, M. L., Gröhn, A. J., Sorensen, C. M., McMurry, P. H., and Pratsinis, S. E., "Mass-mobility characterization of flame-made ZrO2 aerosols: Primary particle diameter and extent of aggregation," *Journal of Colloid and Interface Science*, vol. 387, 2012, pp. 12–23.

[64] Symonds, J. P. R., Reavell, K. S. J., Olfert, J. S., Campbell, B. W., and Swift, S. J., "Diesel soot mass calculation in real-time with a differential mobility spectrometer," *Journal of Aerosol Science*, vol. 38, 2007, pp. 52–68.

[65] TSI, "Product Information: Model 3022A Condensation Particle Counter," 1999.

[66] Kinney, P. D., Pui, D. Y. H., Bryner, N. P., and Mulholland, G. W., "Use of the electrostatic classification method to size 0.1 micrometer SRM particles - A feasibility study," *Journal of Research of the National Institute of Standards and Technology*, vol. 96, 1991, pp. 147–176.

[67] Liscinsky, D. S., and Hollick, H. H., "Effect of particle sampling technique and transport on particle penetration at the high temperature and pressure conditions found in gas turbine combustors and engines," *NASA contractor report, NASA/CR-2010-NNC07CB03C*, 2010.